21

Modelling of Oscillometric Blood Pressure Monitor – from white to black box models

Eduardo Pinheiro and Octavian Postolache
Instituto de Telecomunicações
Portugal

1. Introduction

Oscillometric blood pressure monitors (OBPMs) are a widespread medical device, increasingly used both in domicile and clinical measurements of blood pressure, replacing manual sphygmomanometers due to its simplicity of use and low price. A servo-based air pump, an electronic valve and the inflatable cuff are the main components of an OBPM, the nonlinear behaviour of the device emerges especially from this last element, in view of the fact that the cuff's expansion is constrained (Pinheiro, 2008).

The first sphygmomanometer developments and its final establishment, due to the works of Samuel von Basch, Scipione Riva-Rocci and Nicolai Korotkoff, are over a century old, but still are widely used by trained medical staff (Khan, 2006). In the Korotkoff sounds method, a stethoscope is used to auscultate the sounds produced by the brachial artery while the flow through it starts, after being occluded by the inflation of the cuff. The oscillometric technique is an alternative method which examines the shape of the pressure oscillations that the occluding cuff exhibits when the cuff's pressure diminishes from above systolic to below diastolic blood pressure (Geddes et al., 1982), and in recent times it has been increasingly applied (Pinheiro, 2008).

In the last decades, oscillometric blood pressure monitors have been employed as an indirect measurement of blood pressure, but have not been subject of deep investigation, and have been used as black-box systems, without explicit knowledge of their internal dynamics and features. Bibliography in this field is limited, (Drzewiecki et al., 1993) studied the cuff's mechanics while (Ursino & Cristalli, 1996) have concerned with biomechanical factors of the measurement, but both oblivious to the device's behaviour and performance.

The equations that govern both wrist-OBPM and arm-OPBM behaviour are the same, but wall compliances and other internal parameters assume diverse values, what may also happen between different devices of the same type. The knowledge of the relations ruling the internal dynamics of this instrument will help in the search for improvements in its measurement accuracy and in the device design, given that electronic controllers may be introduced to change the OBPM dynamics improving its sensibility. Moreover, since the OBPM makes discrete measurements of the blood pressure, the understanding of the device's characteristics and dynamics may allow taking a leap towards continuous blood pressure measurement using this inexpensive device.

Analyzing the OBPM, an insightful modelling effort is made to determine a white-box model, describing the dynamics involved in the OBPM during cuff compression and decompression and obtaining several non-ideal and nonlinear dynamics, using the results available on servomotors (Ogata, 2001) and compressible flows (Shapiro, 1953), obtained through electric, mechanic and thermodynamic principles. The approach taken was to divide the OBPM in two subsystems, the electromechanical, which receives electrical supply and outputs a torque in the crankshaft of the air pump, and the pneumatic subsystem, which establishes the evolution of the cuff pressure, separating the compression and decompression phases.
Subsequently blacker-box analysis is presented, in order to provide alternative models that require only the observation of the air pump's electric power dissipation, and pure identification methods to estimate a multiple local model structure. In this last approach the domain of operation was segmented in a number of operating regimes, identifying local models for each regime and fusing them using different interpolation functions thus providing better estimates and more flexibility in the system representation than a single global model (Murray-Smith & Johansen, 1997).

2. White-box model

The main dynamics that characterize the OBPM behaviour are the air pump's response to the command voltage, the air propagation in the device and the inflatable cuff mechanics.

2.1 Electromechanical section

An armature controlled dc servomotor coupled to a crankshaft that manages two cylinders that alternately compress the air are the components of the OBPM's air pump. The servomotor is controlled by V_a, the voltage applied to its armature circuit, while a constant magnetic flux is guaranteed. The armature-winding resistance is labelled R_a, the inductance L_a, and the current i_a, a depiction of the described command circuit is presented in Figure 1.

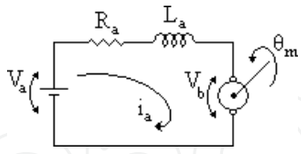

Fig. 1. Servomotor electrical control circuit

Due to the external magnetic field and the relative motion between the motor's armature, the back electromotive force, V_b, appears. At constant magnetic flux V_b is proportional to the motor's angular velocity, ω_m, being related through the back electromotive force constant of the motor, K_1, and with ω_m the derivative of θ_m, the angular displacement of the shaft in the motor, (1).

$$V_b(t) = K_1 \omega_m(t) \tag{1}$$

The current evolution in the circuit, (2), is obtained with Kirchhoff's laws.

$$L_a \frac{di_a(t)}{dt} + R_a i_a(t) + K_1 \omega_m(t) = V_a(t) \tag{2}$$

The transformation from electrical to mechanical energy is done relating the torque τ to the armature current, (3), where K_2 is the motor torque constant.

$$\tau(t) = K_2 i_a(t) \tag{3}$$

Regarding the mechanical coupling to the crankshaft, it will be considered that the servomotor and the crankshaft have moments of inertia J_m and J_c, rotate at angular velocities ω_m and ω_c, and have angular displacements of θ_m and θ_c respectively. The shaft coupling, the motor, and the crankshaft have non-homogeneous stiffness K_3 and viscous-friction b along the shaft (x-axis), Figure 2.

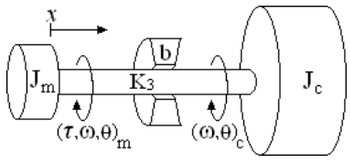

Fig. 2. Mechanical representation of the servomotor coupling to the crankshaft.

The torsion is intrinsically displacement-dependent and the rotational dissipation is velocity-dependent (Ljung & Glad, 1994), so, the equations of torque equilibrium will have to consider the velocity and stiffness in every point of the shaft to compute the torsion, regarding the friction along the shaft. This was dealt computing the product of the mean values of the friction and the angular velocity, which may be piecewise-defined functions. In (4) the angular velocity is defined as a function of time and location in the shaft, $\omega(t,x)$, with $\omega(t,m)$ matching $\omega_m(t)$ and $\omega(t,c)$ matching $\omega_c(t)$.

$$\left\{ \begin{array}{l} J_m \dfrac{d\omega_m(t)}{dt} + \dfrac{\int_m^c b(x)dx \int_m^c \omega(t,x)dx}{(c-m)^2} + \int_m^c K_3(x)\omega(t,x)dx = \tau(t) \\ J_c \dfrac{d\omega_c(t)}{dt} + \dfrac{\int_c^m b(x)dx \int_c^m \omega(t,x)dx}{(c-m)^2} + \int_c^m K_3(x)\omega(t,x)dx = 0 \end{array} \right\} \tag{4}$$

It should be noted that in the case of homogeneous rigidity the last term of the sum is simplified (5) just considering the angular displacements difference between θ_m and θ_c. Moreover, if the coupling between the inertias is perfectly inflexible, which is a good approximation if K_3 is very high, this term disappears.

$$\int_{m}^{c} K_3(x)\omega(t,x)dx = K_3\left[\theta_m(t) - \theta_c(t)\right] \tag{5}$$

Considering that the friction is applied in a single spatial point ($x = b$) and that the rigidity is homogeneous, the set of equations obtained, (4), is linearized to (6).

$$\left\{\begin{array}{l} J_m \dfrac{d\omega_m(t)}{dt} + \dfrac{K_3}{2}\left[\theta_m(t) - \theta_b(t)\right] = \tau(t) \\ b\dfrac{d\theta_b(t)}{dt} + \dfrac{K_3}{2}\left[\theta_b(t) - \theta_m(t)\right] + \dfrac{K_3}{2}\left[\theta_b(t) - \theta_c(t)\right] = 0 \\ J_c \dfrac{d\omega_c(t)}{dt} + \dfrac{K_3}{2}\left[\theta_c(t) - \theta_b(t)\right] = 0 \end{array}\right\} \tag{6}$$

2.2 Pneumatic section

The air pump output flows through a short piping system of circular cross section before entering in the cuff. The cylinders' output is generally composed of a number of orifices with very narrow diameter for example, three orifices with 0.5 mm which are linked through a minor connector to a plastic piping system, of about 5 mm internal diameter, conducing to the cuff. The modelling approach taken considers one-dimensional adiabatic flow, with friction in the ducts, regarding air as a perfect gas, and with the pneumatic connections represented by a converging-diverging nozzle, since the chamber-orifices passage is a contraction, succeed by a two-step expansion, first the passage to the pipes and next the arrival at the cuff.

The assumption of air as a perfect gas means that the specific heat is supposed constant and the relation $p = \rho RT/M$, is considered valid, with R the ideal gas constant, p and T its absolute pressure and temperature, M the gas molar mass and ρ its density. In view of the fact that at temperatures below 282 ºC the error of considering the specific heat constant is negligible, and that deviations from the perfect gas equation of state are also negligible at pressures below 50 atmospheres, the perfect gas approximation is found reasonable, (Shapiro, 1953).

The maximum velocity of the flow, v_{max}, may be determined considering the equation for adiabatic stagnation of a stream (7), where γ is the ratio of specific heats (isobaric over isochoric) and R the air constant, making the absolute temperature T null. It should be noticed that the deceleration's reversibility is not important since the stagnation temperature, T_0, will be the same.

$$v = \sqrt{\frac{2\gamma}{\gamma - 1} R\left(T_0 - T\right)} \tag{7}$$

Regarding the pressure, if the deceleration is irreversible the final pressure will be smaller than the isentropic stagnation pressure, p_0, which is function of the Mach number, M_a, the ratio of the flow velocity and the speed of sound, as seen in (8).

$$p_0 = p\left[1+\left(\frac{\gamma-1}{2}\right)M_a{}^2\right]^{\frac{\gamma}{\gamma-1}} \tag{8}$$

But these are very high limits, if one considers realistic γ, e.g. 1.4 of (Forster & Turney, 1986), even for very low temperature increases, the maximum velocity easily ascends at sonic values, which generates elevated stagnation pressures limits also.

Searching for tighter limits, it is possible to find the characteristics of the air pumps used in these applications. For instance, Koge KPM14A has an inflation time, from 0 to 300 mmHg, in a 100 cm^3 tank, of, about 7.5 seconds. Therefore, considering this inflation time representative, the mean volumetric flow is 13.333 $\times 10^{-6}$ m^3s^{-1} so, the mean air speed is 11.789 ms^{-1} in the three output orifices of the compression chamber, with 0.6 mm of diameter each. The most of the piping has 5 mm of internal diameter, reducing the mean speed to 0.170 ms^{-1}.

The Reynolds number of the flow, $\mathrm{Re} = \rho v D / \mu$, calculated in [20 ; 80] ^oC range to compensate heating of the fluid, considering air's dynamic viscosity μ and density ρ, at these temperatures, and the velocity v in both sections, with different diameter D, will cause the Reynolds number to be between 282 and 392 in the small orifices, and between 41 and 57 in the duct. Hence the Reynolds number is far from 2000, guaranteeing laminar flow in the orifices, even if the effective instantaneous speed achieves five times the mean speed calculated, and in the ducts even if the flow is 35 times faster.

Since the flow is laminar, the friction factor f may be calculated simply using $f = 16/\mathrm{Re}$. The use of the friction factor to represent the walls' shear stress, τ_w, according to $f = 2\tau_w / \rho v^2$, is correct if the flow is steady, but, in cases of velocity profile changes, f represents only an "apparent friction factor" since it also includes momentum-flux effects. In short pipes, which is clearly the case of the OBPM, the average apparent friction factor rises, (Shapiro, 1953) and (Goldwater & Fincham, 1981).

The air is fed into the 5 mm pipes from the three orifices of the compression chamber by an element of unimportant length, which will be assumed frictionless. Since the chamber leads to three 0.6 mm orifices converging to a 1 mm element, which introduces the flow in the 5 mm pipes, the piping profile is converging-diverging.

In view of the fact that the velocity would have to rise almost 29 times to produce sonic flow in the orifices, the flow is considered entirely subsonic, and this piece behaves as a conventional Venturi tube, introducing some losses in the flow (Benedict, 1980), with the flow rate being sensitive to the cuff pressure, what would not happen in the case of sonic or supersonic flow, where shock waves are present (Shapiro, 1953).

The effect of wall friction on fluid properties, considering one-dimensional (dx) adiabatic flow of a perfect gas in a duct with hydraulic diameter D and friction factor f, will rewrite the perfect gas, Mach number, energy, momentum, mass conservation, friction coefficient and isentropic stagnation pressure equations (Shapiro, 1953), creating the system of equations (9). The hydraulic diameter D changes along dx, and these changes must also be included in the model implementation.

$$\begin{cases} \dfrac{dp}{p} = -\dfrac{\gamma M_a{}^2\left[1+(\gamma-1)M_a{}^2\right]}{2\left(1-M_a{}^2\right)}4f\dfrac{dx}{D} \\ \dfrac{dM_a{}^2}{M_a{}^2} = \dfrac{\gamma M_a{}^2\left[2+(\gamma-1)M_a{}^2\right]}{2\left(1-M_a{}^2\right)}4f\dfrac{dx}{D} \\ \dfrac{dv}{v} = \dfrac{\gamma M_a{}^2}{2\left(1-M_a{}^2\right)}4f\dfrac{dx}{D} \\ \dfrac{dT}{T} = -\dfrac{\gamma(\gamma-1)M_a{}^4}{2\left(1-M_a{}^2\right)}4f\dfrac{dx}{D} \\ \dfrac{d\rho}{\rho} = -\dfrac{\gamma M_a{}^2}{2\left(1-M_a{}^2\right)}4f\dfrac{dx}{D} \\ \dfrac{dp_0}{p_0} = -\dfrac{\gamma M_a{}^2}{2}4f\dfrac{dx}{D} \end{cases} \tag{9}$$

The inflatable cuff is an element whose mechanical performance is a determinant factor of the OBPM's response (Pinheiro, 2008). Due to the pressure-volume bond and since the constrictions to the cuff expansion introduce additional dynamics in the OBPM behaviour, the complete model must incorporate (10) the model of cuff's volume evolution with the pressure. It was followed (Ursino & Cristalli, 1996) line of thought, but disagreeing in some particular aspects, since it was considered cuff pressure perfectly equivalent to arm outer surface pressure, greatly reducing the number of biomechanical parameters involved (and their natural discrepancies when changing the subject's characteristics), and also, the ratio of specific heats γ was not considered constant, opposing to other, (Forster & Turney, 1986) and (Ursino & Cristalli, 1996), approaches.

$$\frac{1}{\gamma p_c{}^{1/\gamma}} q^{-1+1/\gamma}\frac{dq}{dt} - \frac{1}{\gamma p_c{}^{1+1/\gamma}} q^{1/\gamma}\frac{dp_c}{dt} = \frac{C_w}{p_c + p_w}\frac{dp_c}{dt} \tag{10}$$

In this equation, q represents the amount of air contained in the cuff, p_c is the cuff pressure (p after the total piping length) expressed in relative units, C_w is the wall compliance, $-p_w$ is the collapse pressure of the cuff internal wall (pressure at which the wall compliance goes infinite).

Finally, having characterized both fluid and structure equations, to complete this fluid-structure interaction model, coupling equations must be defined. One option is to consider fluid velocity inversely dependent on the crankshaft's inertia J_c, or alternatively, to consider that the velocity is dependent on the crankshaft's angular displacement θ_c.

This crankshaft-based coupling is justified taking into consideration the air pump operation cycle. The crankshaft is bicylindrical and each revolution makes the cylinders compress

once, since its construction is symmetrical, each revolution is the execution of the same movement cycle twice, and this cycle can be decomposed in forward (compression) and backward (recovery) movements, thus, the high frequency pulsatile air flow may have its velocity expressed depending only on θ_c or J_c, with an appropriate rational transformation. The modelling exercise is now complete, in the following section a greyer approach to subject is made, studying in more detail the relation of the crankshaft-related variables with the cuff pressure.

2.3 Greyer view – crankshaft load via power dissipation

A simplified way of modelling the mechanic-pneumatic connection will be to consider that all the dynamics of the flow and the inflatable cuff are manifested in the load of the servomotor. This way of thinking has the advantage of being assessed quite easily, by measuring the air pump's power dissipation, or the servomotor's vibrations using strain gages (Schicker & Wegener, 2002), with the latter requiring quite intrusive adjustments in the OBPM, while the first only requires secondary wire connections.

Given that the crankshaft operation cycle can be decomposed in two forward (compressions) and two backward (recoveries) movements, the inertia J_c may be expressed has a function dependent of θ_c, (11), to include the high-frequency dynamics previously described. However, since the dominant effect is unquestionably the filling of the cuff, J_c must be strongly bonded to the cuff pressure. Since it noticeable that the compression takes approximately 3π/4 rad, and the decompression lasts for about π/4 rad, these are the key crankshaft's angular displacement values.

$$J_c(p,\theta_c)=\begin{cases} J_{comp}(p)\left|\sin\left(2\theta_c/3\right)\right|,\ \theta_c\in\left[0,\frac{3\pi}{4}\right]\cup\left[\pi,\frac{7\pi}{4}\right] \\ J_m(p)+J_{dec}(p)\left|\sin\left(2\theta_c-3\pi/2\right)\right|,\ \theta_c\in\left]\frac{3\pi}{4},\pi\right[\cup\left]\frac{7\pi}{4},2\pi\right[\end{cases} \tag{11}$$

The raise in J_c due to the cylinders' forward and backward movement is represented by the terms J_{comp} and J_{dec} correspondingly. The backward movement of the cylinders will add less inertia to J_c than the compression movement, and it is intuitive to suppose that both J_{comp} and J_{dec} will increase when the pressure in the cuff increases. Also, a minimum inertia J_m is added during decompression, since the inertia does not reduce to zero immediately after the compression ends. Subsequent Figure 3 shows the crankshaft's inertia estimative produced by (11) considering one cycle with a J_{comp} value of 0.15 kgm², J_{dec} valuing 0.025 kgm², and J_m 0.045 kgm².

Measurements made on a wrist-OBPM air pump, Koge KPM14A, registered an armature-winding resistance value of 3.9376 Ω and an inductance of 1.5893 mH, using an Agilent 4236B LCR meter (Pinheiro, 2008). Therefore, the implementation of a power measurement scheme based on a 0.111 Ω resistor in series with the supply circuit is innocuous to the OBPM's normal operation. The voltage in this resistor was acquired using a National Instruments DAQ Card 6024E data-acquisition board at a sampling rate of 100 kSamples/second. The power dissipation evolution obtained from these measurements is shown in Figure 4.

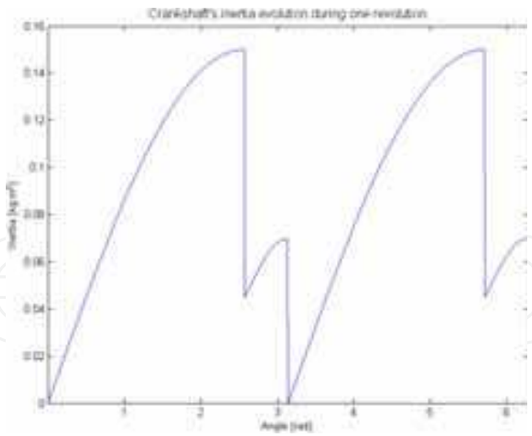

Fig. 3. Crankshaft inertia estimate characterization during one complete revolution, under J_{comp}, J_{dec}, J_m of 0.150, 0.025, and 0.045 kgm².

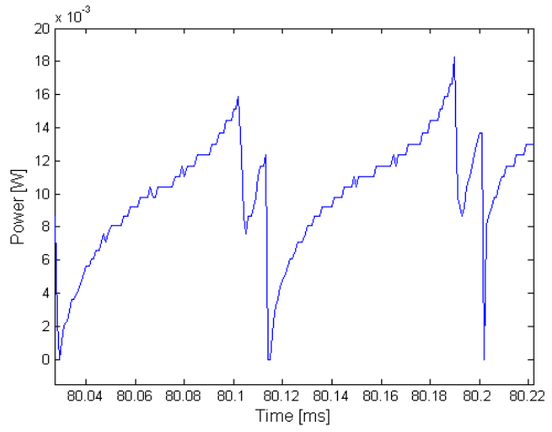

Fig. 4. Power dissipation in the air pump during one complete revolution of the crankshaft.

The abrupt dissipated power decreases after the local maximums are due to the conclusion of the forward and backward movements. The decompression conclusion practically leads to a zero power situation, while the compression conclusion is seen in previous Figure 4 to reduce the power to 50% of the maximum. The 50% proportion is approximately constant if the cuff pressure is below 20 centimetres of mercury column (cmHg), which is the nominal pressure range of OBPM's cuff. This means that in inertia terms, (11), J_m should be half of max{J_{comp}} calculated at the end of the compression.

The cuff pressure directly affects the terms J_{comp} and J_{dec}, since it is the variable ruling the effort of the air pump in each compression. Noticing that it is most important to measure the servomotor's power dissipation evolution and this high-frequency dynamic is not so significant, the curve in Figure 4 may be low-pass filtered in order to evaluate the power evolution once the air pumping changes the cuff pressure, instead of analysing every pump stroke.

To the acquisition hardware was added a Measurement Specialities 1451 pressure sensor, and it was implemented digitally a 3rd order Butterworth low-pass filter with 30 Hz cut-off

frequency. The results obtained are shown in Figure 5, where it is seen the power dissipation curves when compressing to the inflatable cuff, left, and to a constant volume reservoir with about the same capacity, right.

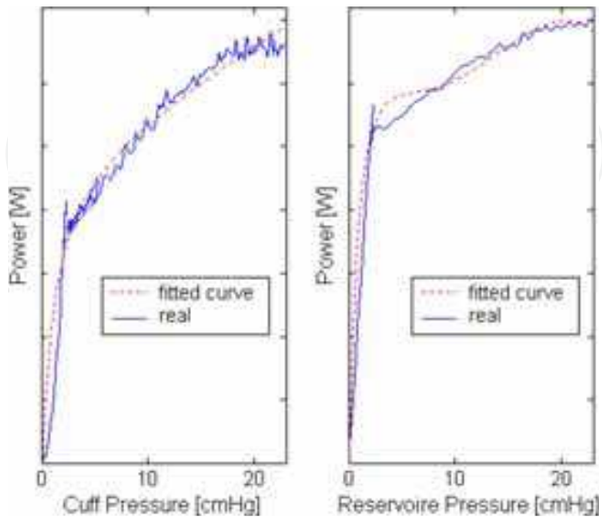

Fig. 5. Air pump's power dissipation dependence of cuff-pressure (blue) and approximating curve (red), when the air pump output is connected to the cuff (left) and to a constant-volume reservoir (right).

The air pump power dissipation, P, relation with the downstream pressure, p, was approximated by a rational function, (12), with coefficient of determination, R^2, of 0.984 when connected to the cuff and 0.967 when connected to the constant-volume reservoir, the a normalized root mean square deviation of the approximations was 2.17% and 2.26%, respectively. With these approximation functions, from the pressure measurements the power dissipation is calculated.

$$P(t) = \frac{a_4 p^4(t) + a_3 p^3(t) + a_2 p^2(t) + a_1 p(t) + a_0}{p(t) + b_0} \tag{12}$$

The inertia of the crankshaft J_c as been described as possible to be estimated from the power dissipation, this makes sense given that the major portion of the crankshaft's inertia is due to the cuff pressure, and the power-pressure relation has been established in (12). Thus, it will be assumed that low-pass filtering the crankshaft's inertia in a 30 Hz 3rd order Butterworth filter Ψ, makes it directly proportional to the power dissipation, (13), being K_4 the power-inertia conversion constant.

$$\Psi\left(J_c(t)\right) = K_4 P(t) \tag{13}$$

Aggregating the equations of the electromechanical section, with (12) and (13), and choosing state vector *X*, defined in (14), it is assembled a greyer and simpler space-state model of the OBPM.

$$X(t)^T = \left[\theta_c(t), \omega_c(t), \theta_m(t), \omega_m(t), i_a(t)\right]^T \tag{14}$$

It should be noticed that since power is the product of i_a the air pump's current (state variable) and V_a the voltage applied (input variable), both pressure and inertia can be estimated knowing only the power and applying (12) and (13) in that order.

2.4 Cuff decompression

The OBPM controls the air pump and the electronic valve in order to pressurize the cuff, until blood flow is cut off, and afterwards slowly reduces the cuff pressure, stopping the compression and letting the cuff's permanent leakage take effect, only opening the electronic valve to swiftly deplete the cuff when the blood pressure measurement is done. During the period while the air pump is stopped and the valve is closed, it is also necessary to evaluate the cuff pressure dynamic when the permanent leakage is the only influence.

In a constant-volume reservoir this dynamic is defined by an exponential decay, as seen in (Lyung & Glad, 1994), in this case, due to the expandability of the cuff, other parameters must infer in the exponential.

It were recorded twelve descents, by turning off the air pump at different pressures, p_{off}, from 9 to 20 cmHg, and then using the DAQ Card 6024E data-acquisition board at 1 kS/s to record the pressure fall curve. It was verified that the cuff pressure had an exponential decay, $p(t) = ae^{-bt}$, and that the exponential function parameters, *a* and *b*, were dependent on the pressure at which the inflation was stopped, p_{0ff}, as presented in (15), with corresponding coefficient of determination values of 0.980 and 0.877.

$$\left\{\begin{array}{l} a = 1.126 p_{off} - 3.35 \\ b = -0.3436 e^{-0.0732 p_{off}} \end{array}\right\} \tag{15}$$

3. Black-box model

The main nonlinearities involved in the OBPM operation refer to the dynamics of the air compression and flow, and the limitations to the cuff expansion. The black-box model approach will define a single-input single-output relation between the voltage supply to the OBPM's air pump, V_a, and the cuff pressure, *p*, applying system identification procedures (Ljung, 1999).

The OBPM, in its normal operating cycle, keeps the electronic valve always closed, by powering it, until cuff depletion is desired, and controls the air pump to compress the cuff until blood stops flowing. To do this, a National Instruments USB-6008 multifunction I/O board was used, with an acquisition rate and generation rate of 50 S/s, together with appropriate circuitry to allow supervision of the device's elements.

The identification procedure consisted of randomly deciding to power the air pump using white noise, but keeping the pressure in a defined range to maintain the device in the operating regime to be identified, thus in case of pressure range surpass the power was shut down and *vice versa*.
It was found by experience that the command voltage should be updated at a rate lower than the 50 S/s used to read the pressure sensor value, to permit the visualization of the effects of the voltage change, and so it was used a 10 S/s output update rate.
Besides connecting the air piping output to the wrist inflatable cuff, the OBPM identification tests were replied in the constant-volume reservoir, to observe the differences in the results due to the reservoir expansion.

3.1 At 5 regimes

The inflatable cuff's maximum nominal pressure is 19.5 cmHg, but, since an hypertensive person may have a systolic blood pressure higher than this limit, the maximum pressure considered was 22 cmHg, and the divisions were: [0 ; 6],]6 ; 10],]10 ; 14],]14 ; 18] and]18 ; 22] cmHg. These divisions arose from the analysis of the OBPM's behaviour when inflating the cuff, from which it was noticed that there are clearly different operating regimes, corresponding to the pressure ranges specified.
The identification tests had 30 minutes of duration, with the first 15 being used to estimate the models and the remaining to validate them. It were computed Output Error (OE), Autoregressive Exogenous Variable (ARX), Autoregressive Moving Average Exogenous Variable (ARMAX), and Box-Jenkins (BJ) models, using the formulation of (Lyung, 1999), of 3rd and 5th order (in all polynomials involved) without delay.
The fits of the various regimes were computed according to (16) (p_{av} is the average pressure and p_{est} the estimated pressure), and respecting the cuff and the constant-volume reservoir, are displayed in Table 1 and Table 2.

$$\text{fit}_{\%} = 100 \times \left| \frac{p_{est} - p}{p - p_{av}} \right| \tag{16}$$

Pressure [cmHg]	OE3	OE5	ARX3	ARX5	ARMAX3	ARMAX5	BJ3	BJ5
0-6	80.56	89.82	75.19	74.96	71.93	87.47	69.47	87.55
6-10	72.20	77.64	66.38	67.82	73.36	77.86	72.47	78.53
10-14	74.09	68.87	62.77	65.78	63.09	75.32	68.95	75.14
14-18	66.64	69.08	51.37	52.68	39.01	36.14	45.86	41.96
18-22	32.34	50.61	33.19	32.77	18.30	13.57	4.39	7.74

Table 1. Models' fit evolution with the air pump output connected to the inflatable cuff

From these results it is seen that the 5th order OE is the fittest model (highest average, μ=71.21, and lowest standard deviation, σ=14.33) with the 3rd order OE having the second highest μ of 65.16, showing the appropriateness of this model type, as it considers the error as white-noise, without estimating a noise model. The global μ is of 59.32 and σ of 25.63.

Pressure [cmHg]	OE3	OE5	ARX3	ARX5	ARMAX3	ARMAX5	BJ3	BJ5
0-6	68.35	68.72	70.78	70.03	68.46	73.79	69.26	69.74
6-10	66.81	70.51	60.50	60.17	60.51	69.01	60.48	71.27
10-14	51.21	51.71	51.57	51.69	58.89	48.06	59.37	60.01
14-18	64.11	62.81	56.22	56.44	57.85	50.85	57.93	51.05
18-22	48.89	9.76	40.00	39.23	3.64	33.78	2.29	36.90

Table 2. Models' fit evolution with the air pump output connected to the constant-volume reservoir

The results presented in Table 2 show the 3rd order OE as being the fittest model (highest μ=59.87, and lowest σ=9.13) while the 5th order BJ has the second highest μ of 57.79. The global μ decreases 9.44% to 53.71 and σ decreases 9.05% to 23.31, implying that although the fits were lower in average, their dispersion also diminished, given the general improvement in the two highest pressure regimes.
It is evident that for both cases the last regime]18 ; 22] cmHg is very difficult to represent using these models, since in the cuff tests the average fit for this regime was of 24.10 and in the reservoir 22.58. This regime is partially above the maximum nominal pressure, and the OBPM's dynamic is not homogeneous inside this pressure range, generating the poorest fit of all regimes.

3.2 At 22 regimes

The pressure range was divided in intervals with 1 cmHg of span, after the first which is [0 ; 2] cmHg, and the tests duration was reduced to 10 minutes. In subsequent Figure 6 and Figure 7 it is displayed the fits evolution, the first presents the results with air pump output connected to the cuff and the latter when connected to the constant-volume reservoir.

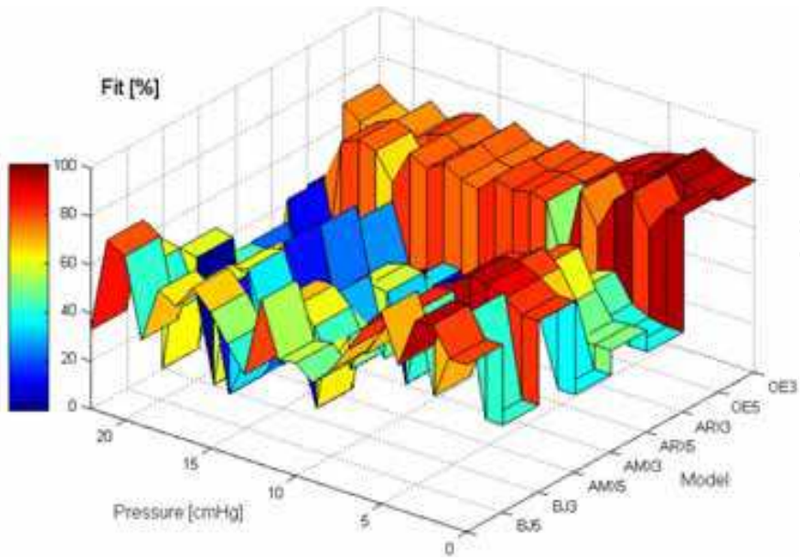

Fig. 6. Models' fit evolution when the air pump output is connected to the cuff

From these results it is seen that the 3rd order OE is the fittest model (highest average, μ=70.60, and lowest standard deviation, σ=6.88) with the 5th order OE having the second highest μ, 64.14. Such results show the suitability of this particular model type, as all other models have worse behaviour, namely the ARX models, with average fit below 30. Comparing with the 5 models approach, the global μ is of 48.61, a decrease of 18.06%, and σ of 26.62, a 3.84% increase.

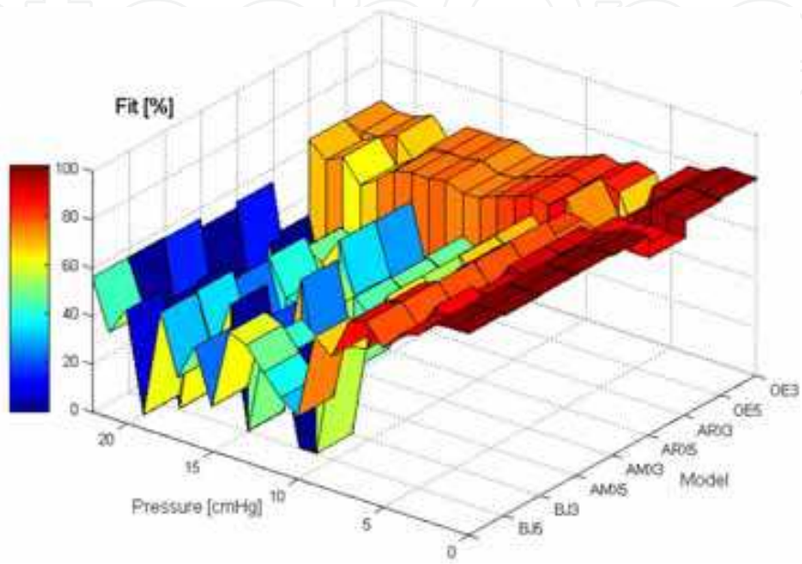

Fig. 7. Models' fit evolution when the air pump output is connected to the constant-volume reservoir

As happened with the cuff tests, the 3rd order OE is again the fittest model (μ_{OE3}=66.64, σ_{OE3}=7.52) while the 5th order OE is very near (μ_{OE5}=65.06). The global μ decreases 5.29% to 50.88 and σ increases 9.05% to 26.79 regarding the 5 models approach. Regarding the compression to the cuff with 22 models, global μ has increased 4.66% and global σ 0.66%.
It is discernible that for both cases the OE models have a regular fit, which does not decrease much in the higher pressure regimes. Moreover, comparing the average fit of the models that comprise the]18 ; 22] cmHg range, to the fit of the corresponding 5-regimes model, the division gains are evident.
Table 3 presents the fit increase for the three best models of the cuff and reservoir tests. The fit increase is the difference from the average fit of the 22-regimes models to the fit of 5-regimes model in the]18:22] cmHg pressure range.

Model	**OE3-cuff**	**OE5-cuff**	**BJ5-cuff**	**OE3-res**	**OE5-res**	**BJ5-res**
Fit increase [%]	31.80	8.01	50.69	11.39	47.55	-1.08

Table 3. Difference between the fit of the]18:22] cmHg regime and the average fits of the models that comprise this pressure range in the 22 divisions tests

3.3 Merging functions

The models correspondent to the different operation regimes should be connected in such way that the information available about a regime is somehow taken into account in a neighbour regime, instead of simply commuting between models (Narendra et al., 1995). To fuse the multiple models identified, a number of different solutions may be tested (Ljung, 2006), in this case, the fusion will be done using linear and Gaussian functions, with and without saturation in the interval centre, Figure 8, varying the dependence on the neighbour models, from the more neighbour-reliant linear without saturation to the most individualist Gaussian with saturation.

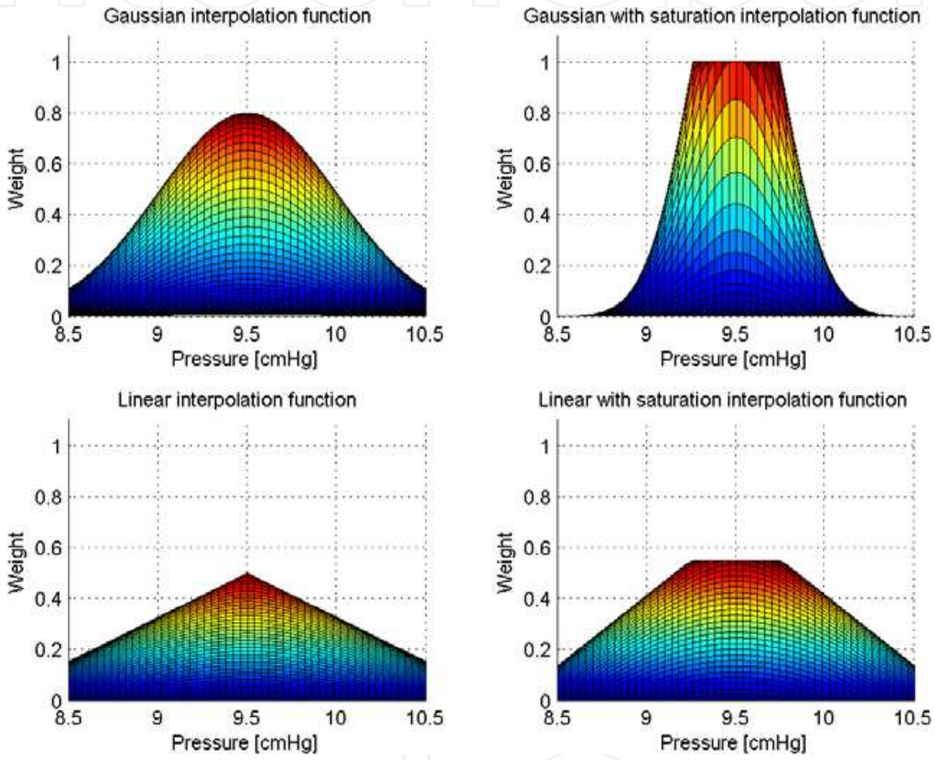

Fig. 8. Interpolation functions used to define the interpolation weights distribution on the global model of the]9 ; 10] cmHg local model, according to the measured pressure

The global model set up to assess the merging functions ability to reproduce the global OBPM behaviour used the 3rd order OE obtained when using 22 pressure divisions, since its fit was always above 60% and with the most homogeneous distribution, and the evaluation tests consisted of 22 trials, which were composed by the first minute of the identification input signal, thus focusing especially in one of the pressure divisions after an initial step input.

The transient response is especially dependent on the fusion quality, as the initial compression traverses many of the local models. The best global performances, regarding mean squared error, were found from 13 to 19 cmHg, Figure 9, although in some experiments the estimates presented overshoot in the transient response, this was rapidly

corrected, and in the remaining of the validation test, the models resemblance to the real behaviour was very truthful.

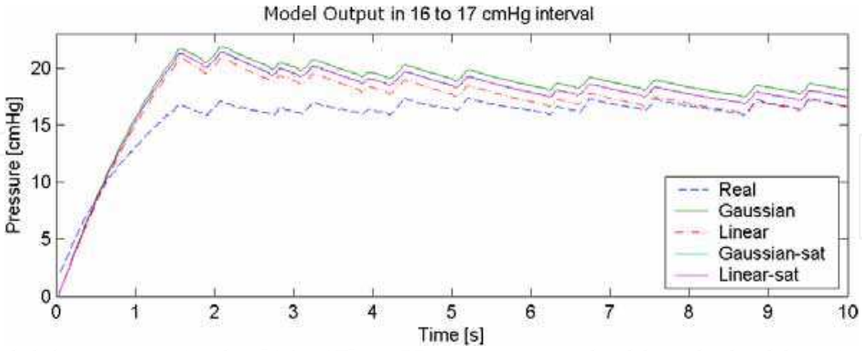

Fig. 9. Models' response in the]16 ; 17] cmHg range test, the blue dashed line is the actual pressure evolution, and the red dash-dot line the linear interpolation estimative, which presents the best transient

The Gaussian function was the most accurate in 10 of the 22 tests, particularly in the lower pressures, the linear and linear with saturation functions were the best solution in 5 tests each, and the Gaussian with saturation only in 2. In the 13 to 19 cmHg range, the linear interpolation function was the most accurate in four intervals, the majority of the cases.

4. Conclusions

A set of equations able to describe in detail the dynamics of an Oscillometric Blood Pressure Monitor, at different depth levels, were considered. Equations fully explaining the electromechanical and pneumatic behaviour of the device have been introduced, but also a more straightforward approach was followed, allowing the assembly of a greyer, yet simpler, model, assuming that the cuff's pressure increase limitations are reflected in the inertia of the air pump's crankshaft, and that this inertia may be estimated from the power dissipation on the air pump. Finally a multiple models identification procedure was described, offering a low computational complexity solution, while completely disregarding the model's physical interpretation, but allowing the compensation of local unsuitabilities while having a consistent global dynamic.

The whiter models developed considered several nonlinearities, such as non-homogeneous stiffness and viscous friction of the servomotor shaft, the flow restrictions in the various piping elements, and the relation between the cuff pressure and its volume. The black-box model approach was also flexible as it is possible to change the models merging functions, as well as the pressure ranges in which the models are used.

After these modelling steps, a number of different tools to obtain an OBPM model was introduced and tested, thus allowing a flexible application of the vast concepts involved in the device's behaviour, to build a model with customisable detail and accuracy. These models may help the search for improvements in the blood pressure measurement accuracy as design changes may improve the OBPM's characteristics, as well as the revision of the components used, to enhance OBPM's dynamics meliorating its performance.

5. Acknowledgements

Eduardo Pinheiro would like to thank the support of *Fundação para a Ciência e Tecnologia*, by means of its SFRH/BD/46772/2008 grant.

6. References

Benedict, R. (1980). *Fundamentals of Pipe Flow*, Wiley & Sons, ISBN 978-0-47-103375-2, New York.

Drzewiecki, G.; Bansal, V.; Karam, E.; Hood, R. & Apple, H. (1993). Mechanics of the occlusive arm cuff and its application as a volume sensor. *IEEE Transactions on Biomedical Engineering,* Vol. 40, No. 7, July 1993, 704-708, ISSN 0018-9294.

Geddes, L. A.; Voelz, M.; Combs, C.; Reiner, D. & Babbs, C. F. (1982). Characterization of the oscillometric method for measuring indirect blood pressure. *Annals of Biomedical Engineering,* Vol. 10, No. 6, November 1982, 271-280, ISSN 0090-6964.

Khan, M. (2006). *Encyclopedia of Heart Diseases*, Academic Press, ISBN 978-0-12-406061-6, USA.

Ljung, L. & Glad T. (1994). *Modeling of Dynamic Systems*. Prentice-Hall, ISBN 978-0-13-597097-3 Englewood Cliffs.

Ljung, L. (1999). *System Identification: Theory for the User (2nd Edition)*. Prentice-Hall, ISBN 978-0-13-656695-3 Englewood Cliffs.

Ljung, L. (2006). Identification of Nonlinear Systems, *Proceedings of the 9th International Conference on Control, Automation, Robotics and Vision*, Plenary paper, ISBN 1-4244-0342 1-06, Singapore, December 2006, IEEE.

Murray-Smith, R. & Johansen, T. (1997). *Multiple Models Approaches to Modelling and Control*. CRC Press, ISBN 978-0-74-840595-4 Boca Raton.

Narendra, K.; Balakrishnan, J.; & Ciliz, M. (1995). Adaptation and Learning Using Multiple Models, Switching and Tuning. *IEEE Control Systems Magazine*, Vol. 15, No. 3, June 1995, 37-51, ISSN 0272-1708.

Ogata K. (2001). *Modern Control Engineering (4th Edition)*, Prentice-Hall, ISBN 978-0-13-060907-6, Englewood Cliffs, New Jersey.

Pinheiro, E. C. (2008). Oscillometric Blood Pressure Monitor Modeling, *Proceedings of the 30th Annual Internacional Conference of the IEEE EMBS*, pp. 303-306, ISBN 978-1-4244-1814-5, Vancouver, August 2008, IEEE.

Shapiro, A. H. (1953). *The Dynamics and Thermodynamics of Compressible Fluid Flow*. Wiley & Sons, ISBN 978-0-47-106691-0, New York.

Schicker, R. & Wegener, G. (2002). *Measuring Torque Correctly*. Hottinger Baldwin Messtechnik, ISBN 978-3-00-008945-9, Darmstadt.

Ursino, M. & Cristalli, C. (1996). A mathematical study of some biomechanical factors affecting the oscillometric blood pressure measurement. *IEEE Transactions on Biomedical Engineering*, Vol. 43, No. 8, August 1996, 761-778, ISSN 0018-9294.

Recent Advances in Biomedical Engineering

Edited by Ganesh R Naik

ISBN 978-953-307-004-9
Hard cover, 660 pages
Publisher InTech
Published online 01, October, 2009
Published in print edition October, 2009

The field of biomedical engineering has expanded markedly in the past ten years. This growth is supported by advances in biological science, which have created new opportunities for development of tools for diagnosis and therapy for human disease. The discipline focuses both on development of new biomaterials, analytical methodologies and on the application of concepts drawn from engineering, computing, mathematics, chemical and physical sciences to advance biomedical knowledge while improving the effectiveness and delivery of clinical medicine. Biomedical engineering now encompasses a range of fields of specialization including bioinstrumentation, bioimaging, biomechanics, biomaterials, and biomolecular engineering. Biomedical engineering covers recent advances in the growing field of biomedical technology, instrumentation, and administration. Contributions focus on theoretical and practical problems associated with the development of medical technology; the introduction of new engineering methods into public health; hospitals and patient care; the improvement of diagnosis and therapy; and biomedical information storage and retrieval. The book is directed at engineering students in their final year of undergraduate studies or in their graduate studies. Most undergraduate students majoring in biomedical engineering are faced with a decision, early in their program of study, regarding the field in which they would like to specialize. Each chosen specialty has a specific set of course requirements and is supplemented by wise selection of elective and supporting coursework. Also, many young students of biomedical engineering use independent research projects as a source of inspiration and preparation but have difficulty identifying research areas that are right for them. Therefore, a second goal of this book is to link knowledge of basic science and engineering to fields of specialization and current research. The editor would like to thank the authors, who have committed so much effort to the publication of this work.

How to reference

In order to correctly reference this scholarly work, feel free to copy and paste the following:

Eduardo Pinheiro and Octavian Postolache (2009). Modelling of Oscillometric Blood Pressure Monitor — from white to black box models, Recent Advances in Biomedical Engineering, Ganesh R Naik (Ed.), ISBN: 978-953-307-004-9, InTech, Available from: http://www.intechopen.com/books/recent-advances-in-biomedical-engineering/modelling-of-oscillometric-blood-pressure-monitor-from-white-to-black-box-models

INTECH
open science | open minds

InTech Europe
University Campus STeP Ri
Slavka Krautzeka 83/A

InTech China
Unit 405, Office Block, Hotel Equatorial Shanghai
No.65, Yan An Road (West), Shanghai, 200040, China

www.intechopen.com

51000 Rijeka, Croatia
Phone: +385 (51) 770 447
Fax: +385 (51) 686 166
www.intechopen.com

中国上海市延安西路65号上海国际贵都大饭店办公楼405单元
Phone: +86-21-62489820
Fax: +86-21-62489821

IntechOpen

IntechOpen